

Robust adaptive position control of automotive electronic throttle valve using PID-type sliding mode technique

Hai Wang · Linfeng Liu · Ping He · Ming Yu ·
Manh Tuan Do · Huifang Kong · Zhihong Man

Received: 17 September 2015 / Accepted: 26 March 2016 / Published online: 6 April 2016
© Springer Science+Business Media Dordrecht 2016

Abstract This paper proposes a robust adaptive position control scheme for automotive electronic throttle (ET) valve. Compared with the conventional throttle control systems, in this paper, a robust adaptive sliding mode (RASM) control scheme is developed in order to eliminate the effects of the parameter uncertainties and nonlinearities including friction, return-spring limp-home and gear backlash. It is shown that both the lumped uncertainty bound and the control gains are adaptively estimated by the update laws, such that not only the bound information of the lumped uncertainty and the control gains are no longer required, but also a robust tracking performance can be ensured in the presence of the parametric variations and disturbances. The comparative simulation and experimental studies are demonstrated to verify the excellent transient and steady-state tracking performance of the proposed RASM controller for ET systems.

Keywords Adaptive sliding mode · Electronic throttle · Lumped uncertainty · Robust tracking

1 Introduction

Electronic throttle (ET) valve systems have been receiving considerable attention of automotive engineers and researchers in the area of vehicle dynamics and control since last two decades [1,2]. Compared with the conventional throttle valve plate in an automotive engine, the ET systems aim at reducing gas emission, providing a better fuel economy and further improving the vehicle drivability. The ET systems are superior to its mechanical counterpart when the control loop fulfils the pre-determined requirements: a fast transient response without overshoot, a high static position precision, easy implementation and strong robustness against the parameter variations and disturbances. However, in practical applications, there exist various types of parameter uncertainties and nonlinearities, i.e., transmission friction, return-spring limp-home (LH), gear backlash and the external disturbance caused by the effect of air flow force. All these uncertain parameter variations and nonlinearities not only significantly enhance the difficulty of the control design, but affect the system performance.

Since the core issue on the performance of ET control systems is the tracking precision and robustness against parameter variations and nonlinearities, a number of researchers have used advanced control methods in the ET control systems for the purpose of ensuring the throttle plate angle to accurately track the reference command. In [3–5], the conventional linear proportional-integral-derivative (PID)

H. Wang (✉) · L. Liu · P. He · M. Yu · H. Kong
Hefei University of Technology, Hefei, Anhui, China
e-mail: wanghai0652@163.com

M. T. Do · Z. Man
Swinburne University of Technology,
Melbourne 3122, Australia

control methods were adopted together with feedforward/feedback compensation for the parameter variations and nonlinearities. However, when the ET system frequently experiences a wide range of parameter variations and nonlinearities, the acceptable tracking performance cannot be ensured. In [6,7], time-optimal control technique was used for the purpose of achieving fast and high-accuracy of reference tracking of throttle plate angle. Nevertheless, since these control methods significantly depend on the modelling accuracy, once large parameter uncertainties and nonlinearities occur leading to the inaccurate system model, the tracking performance and robustness of the ET control system would be deteriorated. Further, several intelligent control methodologies have been used in order to improve the ET control performance particularly under the friction and LH, i.e., neural-network-based ET control and fuzzy control [8–11]. Please note the practical issues are that the adopted back-propagation training algorithm [8,9] may cause slow training and local minima, while the simple fuzzy rules in [10,11] may not fully indicate the working conditions of nonlinear hysteretic ET systems. In [12–15], adaptive control has been applied to ET systems such that the requirement of the system knowledge was successfully relaxed. However, because the system identification of the main component was first used, followed by the adaptively update for the process parameters, the system performance may be affected if large parameter uncertainties and nonlinearities exist resulting in the inaccurate system identification. From the robustness point of view, sliding mode control [16–27] and observer techniques were employed in the ET systems, such that the effects of the parametric variations and nonsmooth nonlinearities can be alleviated [28,29]. However, how the uncertainty bound can be appropriately obtained without causing control saturation is still challenging.

Motivated by the advantages of both adaptive control and sliding mode control methods, in this paper, we develop a PID-type sliding mode-based adaptive control scheme for adaptively estimating both the lumped uncertainty bound and the control gains in Lyapunov sense. Thus, not only the influences of the lumped uncertainty can be alleviated, but also the PID-type sliding mode control gains are adaptively adjusted for both transient and steady-state tracking purpose based on the closed-loop tracking error. It will be shown from the simulation results that the proposed control scheme exhibits an excellent tracking performance

in terms of the step and sinusoidal reference commands. Also, the strong robustness against the parameter variations, nonlinearities and external disturbance is guaranteed.

The rest of this paper is organized as follows: In Sect. 2, the dynamic model of ET systems is presented and the expression of the bounded lumped uncertainty is provided. In Sect. 3, a robust adaptive sliding mode (RASM) controller is developed where the lumped uncertainty bound and sliding mode control gains are both adaptively estimated based on the designed update laws, and the asymptotic error convergence as well as the closed-loop error convergence analysis is discussed. Finally, Sects. 4 and 5 present the simulation and experimental results for verifying the remarkable reference tracking characteristic of the proposed RASM control. Section 6 gives the conclusion and some further work.

2 Problem formulation

The architecture of an ET control system is shown in Fig. 1 [15,19]. It is clearly seen that the ET system involves the following parts: an accelerator pedal, a microcontrol unit (MCU), a DC motor, a throttle valve plate, a reduction gear set including a motor pinion gear, an intermediate gear, and a sector gear, respectively, two nonlinear return springs, and two position sensors for measuring the pedal movement and the actual throttle position, respectively.

When the accelerator pedal is pressed down by the driver, the reference command for the throttle valve to track is first measured by the pedal position sensor and then sent to the MCU in Engine Management System for the purpose of determining the appropriate air-fuel mixture to be fed into the engine. Also, the actual throttle opening is measured by the throttle position sensor. The control voltage provided by the MCU with the help of PWM control module, is to power the DC motor and

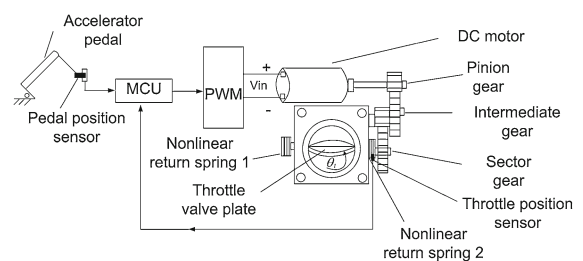


Fig. 1 ET system model

generate the rotational torque. As a result, the actual throttle opening is obtained or maintained, through the reduction gear set, to follow the desired opening angle.

Considering the fact that the armature current dynamics can be neglected resulting from the small value of armature inductance, the system dynamics of the ET valve and the DC motor are given by [9, 15]:

$$J_m \dot{\omega}_m = \tau_a - B_m \omega_m - \tau_m \tag{1}$$

$$\tau_a = k_t \frac{u - k_e \omega_m}{R} \tag{2}$$

$$J_t \dot{\omega}_t = \tau_l - B_t \omega_t - \tau_f - \tau_{sp} - \tau_L \tag{3}$$

where J_m and J_t are the moments of inertia of the motor and throttle valve, respectively, B_m and B_t are the viscous damping coefficients of the motor and throttle valve, respectively, ω_m and ω_t are angular velocities of the motor and throttle plate, satisfying $\omega_m = N\omega_t$ with N defined as the gear ratio, k_t and k_e are the constants of motor torque and electromotive force, respectively, τ_a is the motor torque, τ_m and τ_l are the gear input and output torque, τ_f is the friction torque, τ_{sp} is the return-spring torque, τ_L is the load disturbance torque resulting from the effect of the air flow force applying on the throttle plate, R is the total resistance of the armature circuit, u is the control input voltage.

Although many types of friction exist in the motion of throttle plate including Coulomb, viscous and rising static friction, the following Coulomb friction model is only considered in this paper for the simplicity:

$$\tau_f = F_s \text{sign}(\omega_t) \tag{4}$$

with F_s the Coulomb friction constant and $\text{sign}(\omega_t)$ the sign function expressed as:

$$\text{sign}(\omega_t) = \begin{cases} 1 & \text{for } \omega_t > 0 \\ 0 & \text{for } \omega_t = 0 \\ -1 & \text{for } \omega_t < 0 \end{cases} \tag{5}$$

The throttle return-spring torque is given by the following nonlinear function

$$\begin{aligned} \tau_{sp} &= \begin{cases} \tau_{LH} + k_{sp}(\theta_t - \theta_0), & \theta_0 < \theta_t < \theta_{max} \\ -\tau_{LH} - k_{sp}(\theta_0 - \theta_t), & \theta_{min} < \theta_t < \theta_0 \end{cases} \\ &= \tau_{LH} \text{sgn}(\theta_t - \theta_0) \\ &\quad + k_{sp}(\theta_t - \theta_0), \theta_{min} < \theta_t < \theta_{max} \end{aligned} \tag{6}$$

where k_{sp} is the spring elastic coefficient, τ_{LH} is the spring offset, θ_t is the opening angle of the ET plate and thus $\dot{\theta} = \omega_t$, θ_0 is the default opening angle of the throttle plate, which is also called the LH position, θ_{min} and

θ_{max} are the minimum and maximum opening angles of the throttle plate, respectively.

Due to the fact that three gears exist in the ET valve in order to transfer the torque from the motor to the valve plate, the backlash nonlinearity between gears is generally expressed as

$$\tau_l(t) = \begin{cases} N(\tau_m - \delta), & \dot{\tau}_m > 0 \text{ and } \tau_l = N(\tau_m(t) - \delta) \\ N(\tau_m + \delta), & \dot{\tau}_m < 0 \text{ and } \tau_l = N(\tau_m(t) + \delta) \\ \tau(t_-), & \text{otherwise} \end{cases} \tag{7}$$

where δ is the backlash distance, $\tau_l(t_-)$ indicates that there is no change in $\tau_l(t)$.

For the controller design, it is worth noting that the backlash model in (7) can be further described by [15]

$$\tau_l(t) = N\tau_m(t) + d(\tau_m(t)) \tag{8}$$

where $d(\cdot)$ is a bounded nonlinear function regarding $\tau_m(t)$ and $\dot{\tau}_m(t)$ such that, $|d(\tau_m(t))| \leq \bar{d}$, where \bar{d} is the corresponding upper bound.

As a result, using (1) and (2) in (3) by eliminating ω_m , the aforementioned dynamic equations of the ET control system can be simplified as

$$J_{eq} \dot{\omega}_t \left(B_{eq} + \frac{k_t k_e}{R} N^2 \right) \omega_t + \tau_f + \tau_{sp} - \tau_D = \frac{Nk_t}{R} u \tag{9}$$

where J_{eq} and B_{eq} are the equivalent inertia and damping coefficient of the ET system model, respectively, which are defined as

$$J_{eq} = N^2 J_m + J_t \tag{10}$$

$$B_{eq} = B_t + N^2 B_m \tag{11}$$

and τ_D is the generalized bounded disturbance torque, which is given by

$$\tau_D = d(\tau_m) - \tau_L \tag{12}$$

where τ_D is bounded by

$$|\tau_D| \leq \rho \tag{13}$$

where ρ is a positive constant. Let

$$a = \frac{J_{eq} R}{Nk_t} \tag{14}$$

$$b = \frac{\left(B_{eq} + \frac{k_t k_e}{R} N^2 \right) R}{Nk_t} \tag{15}$$

$$\tau_{fa} = \frac{F_s \text{sign}(\omega_t) R}{Nk_t} \tag{16}$$

$$\tau_{spa} = \frac{[\tau_{LH0} \text{sgn}(\theta_t - \theta_0) + k_{sp}(\theta_t - \theta_0)] R}{Nk_t} \tag{17}$$

$$\tau_{Da} = \frac{\tau_D R}{Nk_t} \tag{18}$$

We can rewrite (9) in the form of throttle position θ_t as

$$a\ddot{\theta}_t + b\dot{\theta}_t + \tau_{fa} + \tau_{spa} - \tau_{Da} = u \tag{19}$$

Taking into account the uncertainties, we express (14)–(17) as:

$$a = a_0 + \Delta a \tag{20}$$

$$b = b_0 + \Delta b \tag{21}$$

$$\tau_{fa} = \tau_{fa0} + \Delta \tau_{fa} \tag{22}$$

$$\tau_{spa} = \tau_{spa0} + \Delta \tau_{spa} \tag{23}$$

where $a_0 = \frac{J_{eq0} R_0}{N_0 k_{r0}}$, $b_0 = \frac{(B_{eq0} + \frac{k_{t0} k_{e0}}{R_0} N_0^2) R_0}{N_0 k_{r0}}$, J_{eq0} , B_{eq0} , N_0 , k_{r0} , k_{e0} , and R_0 are the nominal values of the system parameters, $\tau_{fa0} = \frac{F_s \text{sign}(\omega_t) R_0}{N_0 k_{r0}}$, $\tau_{spa0} = \frac{[\tau_{LH0} \text{sgn}(\theta_t - \theta_0) + k_{sp0}(\theta_t - \theta_0)] R_0}{N_0 k_{r0}}$ are the nominal values of friction and return-spring torque disturbances, Δa , Δb , $\Delta \tau_{fa} = \Delta_1 \text{sign}(\omega_t)$, $\Delta \tau_{spa} = [\Delta_2 \text{sgn}(\theta_t - \theta_0) + \Delta_3 \theta_t - \Delta_4]$, Δ_i ($i = 1, 2, 3, 4$) denote the unknown bounded uncertainties of the system coefficients.

Now, (19) can be written as:

$$a_0 \ddot{\theta}_t + b_0 \dot{\theta}_t + \tau_{fa0} + \tau_{spa0} = u + \tau_{lum} \tag{24}$$

where τ_{lum} represents the total lumped uncertainty of ET as follows:

$$\tau_{lum} = -\Delta a \ddot{\theta}_t - \Delta b \dot{\theta}_t - \Delta \tau_{fa} - \Delta \tau_{spa} + \tau_{Da} \tag{25}$$

and τ_{lum} is bounded by a positive constant η such that

$$|\tau_{lum}| \leq \eta \tag{26}$$

Thus, we have the following nominal system model:

$$a_0 \ddot{\theta}_t + b_0 \dot{\theta}_t + \tau_{fa0} + \tau_{spa0} = u_{nom} \tag{27}$$

where u_{nom} is the nominal control signal.

Remark 1 It is easily seen from (25) that, the lumped uncertainty of the ET system in (24) consists of the

parameter uncertainties in the DC motor and the valve plate, and the estimation errors of the Coulomb friction torque and the throttle return-spring torque, and the uncertain disturbances including load torque and the gear backlash nonlinearity. In reality, it is difficult to obtain the bound information of the lumped uncertainty due to the high complexity of the uncertainty structure and thus it is essential that the uncertainty bound can be online estimated for the purpose of eliminating the effects of the lumped uncertainty.

3 Design of RASM control scheme

In this section, an RASM control scheme is designed for eliminating the effects of the system lumped uncertainty such that the ET plate angle can track the desired reference signal θ_{des} with a satisfactory performance, i.e., transient performance (settling time and overshoot), steady-state error, and robustness with respect to parameter variations and external disturbances.

First, the tracking error between the actual ET opening angle θ_t and the reference angle θ_{des} is defined as:

$$\varepsilon_\theta = \theta_t - \theta_{des} \tag{28}$$

Given the system model in (24), we have the error dynamics of the closed-loop ET system as follows:

$$\ddot{\varepsilon}_\theta = -\frac{b_0}{a_0} \dot{\theta}_t + \frac{u - \tau_{fa0} - \tau_{spa0}}{a_0} + \frac{\tau_{lum}}{a_0} - \ddot{\theta}_{des} \tag{29}$$

In order to use the sliding mode technique in the control design for achieving the aforementioned performance indexes, we adopt the following PID-type sliding variable:

$$s = \dot{\varepsilon}_\theta + \hat{\Lambda}_1 \varepsilon_\theta + \hat{\Lambda}_2 \int_0^t \varepsilon_\theta(\tau) d\tau \tag{30}$$

where $\hat{\Lambda}_1$ and $\hat{\Lambda}_2$ are two control gains to be online estimated by the corresponding adaptive laws.

Then, the RASM control design and the convergence analysis of the closed-loop error dynamics of the ET system are given in the following theorem.

Theorem 1 *Considering the ET system in (24) with the error dynamics in (29), the output position tracking error ε_θ will asymptotically converge to zero if the control law is designed such that*

$$\begin{aligned}
 u &= \tau_{\text{fa}0} + \tau_{\text{spa}0} + (b_0 - a_0 \hat{\Lambda}_1) \dot{\theta}_t \\
 &+ a_0 \left(\ddot{\theta}_{\text{des}} + \hat{\Lambda}_1 \dot{\theta}_{\text{des}} + \hat{\Lambda}_2 \theta_{\text{des}} \right) \\
 &- a_0 \hat{\Lambda}_2 \theta_t - \hat{\eta} \text{sign}(s) - ks \tag{31}
 \end{aligned}$$

where k is a designed control parameter for the reaching phase of the sliding mode, $\hat{\eta}$ is the online estimated bound of the lumped uncertainty bound η , $\hat{\Lambda}_1$ and $\hat{\Lambda}_2$ are two estimated control gains, according to the following update laws:

$$\dot{\hat{\eta}} = \xi_1 |s| \tag{32}$$

$$\dot{\hat{\Lambda}}_1 = -\xi_2 s \varepsilon_\theta \tag{33}$$

$$\dot{\hat{\Lambda}}_2 = -\xi_3 s \int_0^t \varepsilon_\theta(\tau) d\tau \tag{34}$$

Proof Consider a Lyapunov function $V = \frac{a_0}{2} s^2 + \frac{\xi_1^{-1}}{2} (\hat{\eta} - \eta)^2$ and taking the time derivative of V , we obtain

$$\begin{aligned}
 \dot{V} &= a_0 s \dot{s} + \xi_1^{-1} (\hat{\eta} - \eta) \dot{\hat{\eta}} \\
 &= a_0 s \left(\ddot{\theta} + \hat{\Lambda}_1 \dot{\varepsilon}_\theta + \hat{\Lambda}_2 \varepsilon_\theta + \dot{\hat{\Lambda}}_1 \varepsilon_\theta \right. \\
 &\quad \left. + \dot{\hat{\Lambda}}_2 \int_0^t \varepsilon_\theta(\tau) d\tau \right) + \xi_1^{-1} (\hat{\eta} - \eta) \dot{\hat{\eta}} \\
 &= a_0 s \left(-\frac{b_0}{a_0} \dot{\theta}_t + \frac{u - \tau_{\text{fa}0} - \tau_{\text{spa}0}}{a_0} + \frac{\tau_{\text{lum}}}{a_0} \right. \\
 &\quad \left. - \ddot{\theta}_{\text{des}} + \hat{\Lambda}_1 \dot{\varepsilon}_\theta + \hat{\Lambda}_2 \varepsilon_\theta \right) + a_0 s \dot{\hat{\Lambda}}_1 \varepsilon_\theta \\
 &\quad + a_0 s \dot{\hat{\Lambda}}_2 \int_0^t \varepsilon_\theta(\tau) d\tau + \xi_1^{-1} (\hat{\eta} - \eta) \dot{\hat{\eta}} \\
 &= s \left[-b_0 \dot{\theta}_t + u - \tau_{\text{fa}0} - \tau_{\text{spa}0} + \tau_{\text{lum}} - a_0 \ddot{\theta}_{\text{des}} \right. \\
 &\quad \left. + a_0 \hat{\Lambda}_1 (\dot{\theta}_t - \dot{\theta}_{\text{des}}) + a_0 \hat{\Lambda}_2 (\theta_t - \theta_{\text{des}}) \right] \xi_1^{-1} (\hat{\eta} - \eta) \dot{\hat{\eta}} \\
 &\quad + a_0 s \dot{\hat{\Lambda}}_1 \varepsilon_\theta + a_0 s \dot{\hat{\Lambda}}_2 \int_0^t \varepsilon_\theta(\tau) d\tau \\
 &= s \left[(-b_0 + a_0 \hat{\Lambda}_1) \dot{\theta}_t - a_0 (\ddot{\theta}_{\text{des}} + \hat{\Lambda}_1 \dot{\theta}_{\text{des}} \right. \\
 &\quad \left. + \hat{\Lambda}_2 \theta_{\text{des}}) + a_0 \hat{\Lambda}_2 \theta_t + u - \tau_{\text{fa}0} - \tau_{\text{spa}0} \right. \\
 &\quad \left. + \tau_{\text{lum}} \right] + \xi_1^{-1} (\hat{\eta} - \eta) \dot{\hat{\eta}} \\
 &\quad + a_0 s \dot{\hat{\Lambda}}_1 \varepsilon_\theta + a_0 s \dot{\hat{\Lambda}}_2 \int_0^t \varepsilon_\theta(\tau) d\tau \\
 &= -\hat{\eta} |s| + \tau_{\text{lum}} s - ks^2 + \xi_1^{-1} (\hat{\eta} - \eta) \dot{\hat{\eta}} \\
 &\quad + a_0 s \dot{\hat{\Lambda}}_1 \varepsilon_\theta + a_0 s \dot{\hat{\Lambda}}_2 \int_0^t \varepsilon_\theta(\tau) d\tau
 \end{aligned}$$

$$\begin{aligned}
 &= -\hat{\eta} |s| + \tau_{\text{lum}} s - ks^2 + \xi_1^{-1} (\hat{\eta} - \eta) \xi_1 |s| \\
 &\quad - a_0 \xi_2 s^2 \varepsilon_\theta^2 - a_0 \xi_3 s^2 \left(\int_0^t \varepsilon_\theta(\tau) d\tau \right)^2 \\
 &= \tau_{\text{lum}} s - \eta |s| - ks^2 - a_0 \xi_2 s^2 \varepsilon_\theta^2 \\
 &\quad - a_0 \xi_3 s^2 \left(\int_0^t \varepsilon_\theta(\tau) d\tau \right)^2 \\
 &\leq -|s| (\eta - |\tau_{\text{lum}}|) - ks^2 - a_0 \xi_2 s^2 \varepsilon_\theta^2 \\
 &\quad - a_0 \xi_3 s^2 \left(\int_0^t \varepsilon_\theta(\tau) d\tau \right)^2 \\
 &\leq -\sigma |s| < 0 \quad \text{for } |s| \neq 0 \tag{35}
 \end{aligned}$$

where σ is a positive constant that can always be found satisfying $\eta - \max\{|\tau_{\text{lum}}|\} \geq \sigma$. Expression (35) ensures that the sliding variable s reaches the sliding mode surface $s = 0$ in a finite time [19]. Thus, the error dynamics of the closed-loop ET system exponentially converges to zero on the sliding mode surface.

Remark 2 It has been seen from the control law in (31) that the control parameters k and ξ_i ($i = 1, 2, 3$) play an important role in ensuring a remarkable control performance. Thus, the control parameters should be properly chosen and the selection criteria are given as follows: (i) The parameter k is designed for controlling the convergence of the sliding variable in the reaching phase, however, it cannot be too large in order to avoid the control saturation. (ii) It is observed from the above stability proof that the adaption rates ξ_i ($i = 1, 2, 3$) determine the closed-loop convergence performance and thus should be carefully selected.

Remark 3 It should be noted that the pre-determined two constant gains $\hat{\Lambda}_1$ and $\hat{\Lambda}_2$ in [3] may not be optimal for the both cases of step and sinusoidal reference inputs, which may increase the oscillations and introduce high-frequency unmodeled dynamics in the ET control system. In addition, the well-tuned gains can ensure an acceptable tracking performance in normal operating conditions. However, once large parameter variations and nonlinearities of ET systems occur, the control gains are no longer optimal such that both the robustness and the tracking performance will be deteriorated. As a result, we adopt the adaptive laws for updating the variable gains in order to avoid the above issues.

Remark 4 Due to the signum function $\text{sign}(s)$ included in the RASM control in (31), the chattering phenomenon occurs in the control signal. This chattering issue

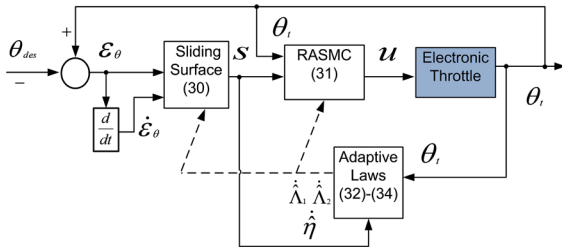


Fig. 2 Control diagram of ET system

can be tackled by using the following boundary-layer RASM (BRASM) control method:

$$u = \tau_{fa0} + \tau_{spa0} + (b_0 - a_0 \hat{\Lambda}_1) \dot{\theta}_t + a_0 (\ddot{\theta}_{des} + \hat{\Lambda}_1 \dot{\theta}_{des} + \hat{\Lambda}_2 \theta_{des}) - a_0 \hat{\Lambda}_2 \theta_t - \hat{\eta} \text{sat}(s) - ks \tag{36}$$

where $\text{sat}(s)$ is the saturation function defined as:

$$\text{sat}(s) = \begin{cases} \frac{s}{\xi_4} & \text{for } |s| < \xi_4 \\ \text{sign}(s) & \text{for } |s| \geq \xi_4 \end{cases} \tag{37}$$

where $\xi_4 > 0$ denotes the boundary-layer thickness ensuring that s is bounded by ξ_4 . Please note that, although the closed-loop error dynamics of the ET system with the BRASM control in (36) cannot have a zero-error convergence, through the appropriate selection of the positive constant ξ_4 , the tracking error remains ultimately bounded within a neighborhood of the sliding mode surface, which satisfies the tracking precision requirement in practice.

The complete control diagram of the ET system is summarized in Fig. 2 and the tracking performance of the proposed RASM control will be validated by simulation studies in the following section.

4 Simulation results and discussion

In order to verify the efficacy and advantages of the proposed RASM control for the ET system, a few computer simulations are carried out in comparison with the traditional PID control and the H_∞ control, respectively.

4.1 Simulation environment and parameter setting

In practical applications, since the ET system often experiences sudden changes from large to small opening angles or vice versa, parametric variations and

Table 1 Nominal parameters of ET system [15]

Parameter	Value
a_0	0.063
b_0	0.616
k_{r0} (Nm s/rad)	0.0185
k_{e0} (V s/rad)	0.0285
k_{sp0} (Nm/rad)	0.087
τ_{LH0} (m)	0.396
R_0 (Ω)	1.15
F_{s0} (m)	0.284
L (mH)	1.5
θ_0 ($^\circ$)	12
N_0	20.68

external disturbances. Thus, we adopt the following two cases in simulation (20 s) for demonstrating the validity and excellent performance of the proposed RASM control.

Case 1 Note that the reference command θ_{des} is a combination of step signals with different amplitudes through the LH position θ_0 such that the fast transient performance can be evaluated. In addition, the external load disturbance $\tau_L = 0.1 \sin(2\pi t)$ Nm and the 10% parametric variations in (14)–(17) are both considered.

Case 2 The reference command is a periodical sinusoidal signal $\theta_{des} = 35 + 5\sin(\pi t)$ ($^\circ$). The external load disturbance $\tau_L = 0.1 \sin(2\pi t)$ Nm and the 10% parametric variations in (14)–(17) are also considered when simulation starts in order to test the control robustness.

For the comparison purpose, the PID control with feed-forward compensation [3] and the H_∞ control laws [30] are given as follows:

$$u_{PID} = -5e - 1.2 \int_0^t e d\tau - 0.1\dot{e} + \tau_{fa0} + \tau_{spa0} \tag{38}$$

$$u_{H_\infty} = 0.15\ddot{\theta}_{des} + 0.5\dot{\theta}_t - 14e - 0.6\dot{e} \tag{39}$$

Note that the H_∞ controller is designed optimally for minimizing the effects of parameter uncertainties and disturbances and achieving a bounded tracking error. The values of the nominal parameters of the ET system in (24) are listed in Table 1 [15]. The parameters of the proposed RASM control scheme for the ET

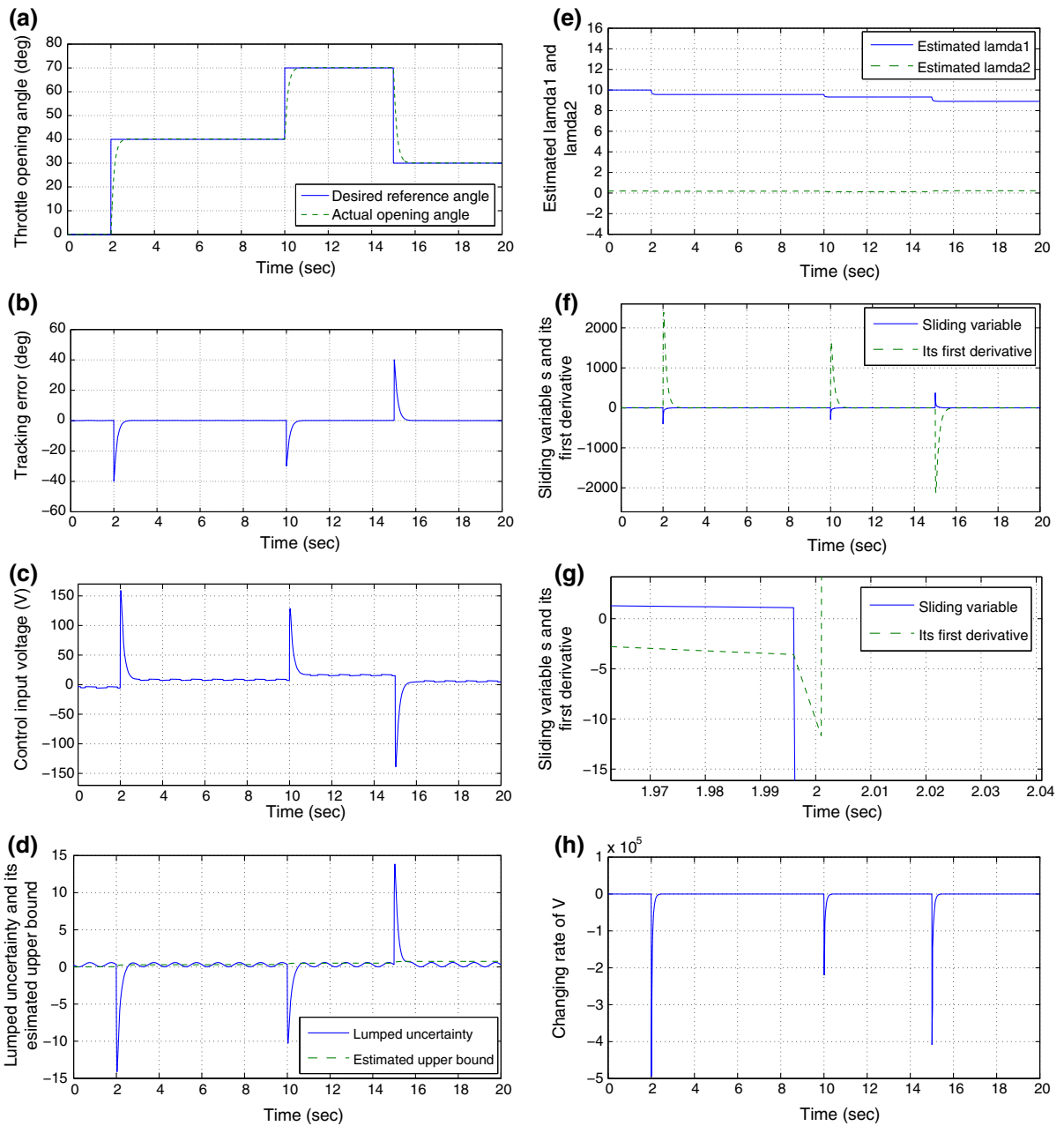


Fig. 3 Control performance of RASM control in Case 1. **a** Tracking performance. **b** Tracking error. **c** Control voltage. **d** Lumped uncertainty and its estimated upper bound. **e** Estimated gains $\hat{\lambda}_1$

and $\hat{\lambda}_2$. **f** Sliding variable s and its first derivative. **g** First derivative of sliding variable at time 2 s (zoom in). **h** Changing rate of Lyapunov function V

system are chosen as: $k = 0.3, \xi_1 = 0.0063, \xi_2 = \xi_3 = 0.001, \xi_4 = 0.3$. The initial values of the estimated parameters are set as $\hat{\lambda}_1(0) = 10, \hat{\lambda}_2(0) = 0.2, \hat{\eta}(0) = 0.001$. The sampling period is chosen as $\Delta T = 0.005s$. Then, the RASM control law in (31) is given by:

$$\begin{aligned}
 u_{\text{RASM}} = & \tau_{\text{fa}0} + \tau_{\text{s pa}0} + \left(0.616 - 0.063\hat{\lambda}_1\right) \dot{\theta}_t \\
 & + 0.063 \left(\ddot{\theta}_{\text{des}} + \hat{\lambda}_1 \dot{\theta}_{\text{des}} + \hat{\lambda}_2 \theta_{\text{des}}\right) \\
 & - 0.063\hat{\lambda}_2 \theta_t - \hat{\eta} \text{sign}(s) - 0.15s \quad (40)
 \end{aligned}$$

where $\hat{\lambda}_1, \hat{\lambda}_2$, and $\hat{\eta}$ are given in (32)–(34).

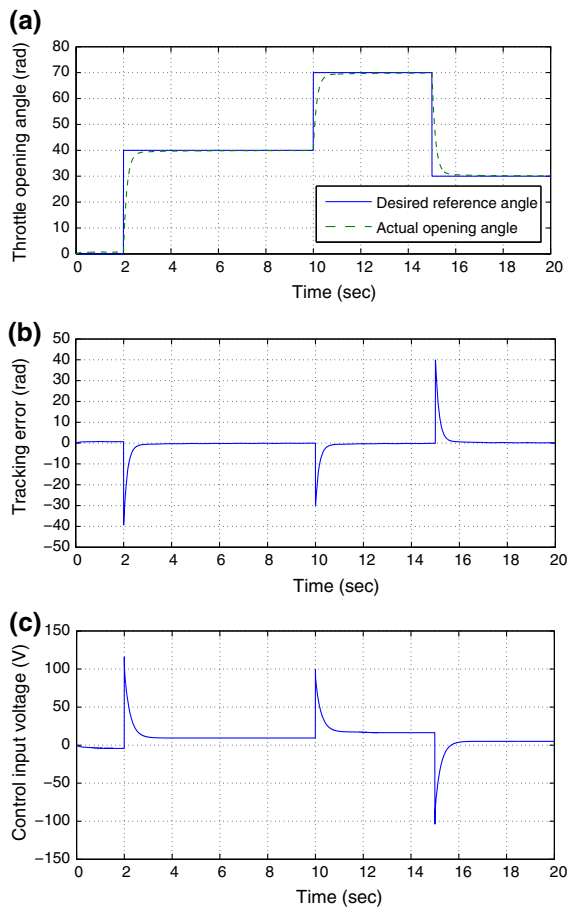


Fig. 4 Control performance of PID control in Case 1. **a** Tracking performance. **b** Tracking error. **c** Control voltage

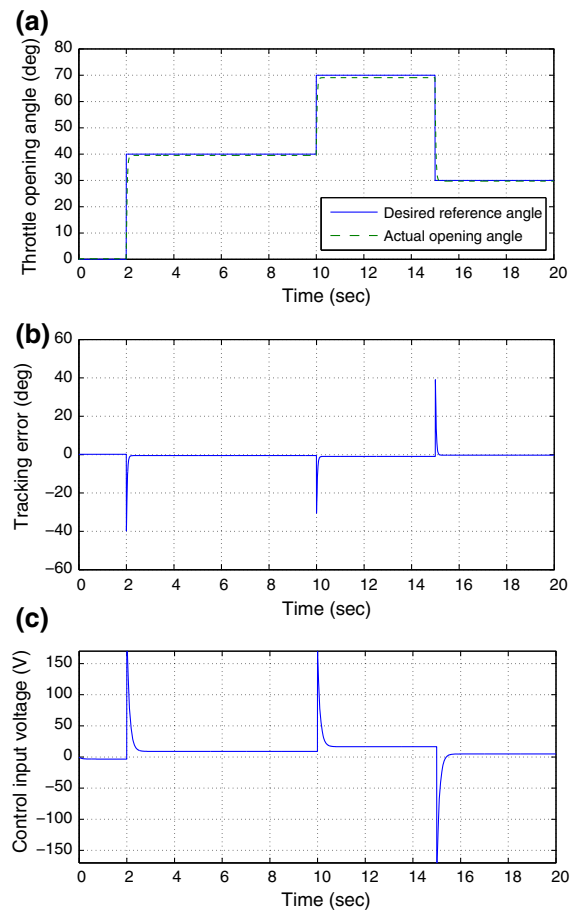


Fig. 5 Control performance of H_∞ control in Case 1. **a** Tracking performance. **b** Tracking error. **c** Control voltage

4.2 Simulation results

Figure 3 shows the throttle tracking performance of the proposed RASM control under set-point regulation in Case 1. It can be seen from Fig. 3a, b that, the actual throttle opening angle is able to closely track the reference command, with the settling time around 0.4s and almost zero steady-state error during the whole period, which perfectly meets the requirement of both the transient and steady-state tracking. Moreover, the online estimated bound of the lumped uncertainty $\hat{\eta}$, and the control gains $\hat{\Lambda}_1$ and $\hat{\Lambda}_2$ are shown in Fig. 3d, e, respectively. It should be noted that all of the three parameters are adaptively adjusted in Lyapunov sense for ensuring the closed-loop stability and it is unnecessary for them to converge to their real values. It is seen from Fig. 3f, g that, at each throttle change

period, the sliding variable s and its changing rate are driven by the proposed control to converge to zero at a very fast convergence rate such that the closed-loop stability can be guaranteed. In particular, it is noted from Fig. 3g that the changing rate of the sliding variable \dot{s} at time 2s is negative, which keeps consistency with the decreasing trend of the sliding variable shown in Fig. 3f. The cases of \dot{s} at time 10 and 15s are similar to the one at time 2s and thus here is omitted. In addition, Fig. 3h shows that the changing rate of the Lyapunov function \dot{V} is always non-positive, indicating the stability of the closed-loop error dynamics under the changes of the reference commands, parameter variations and external disturbances.

For the comparison purpose, Figs. 4 and 5 show the time responses of the throttle opening angles and track-

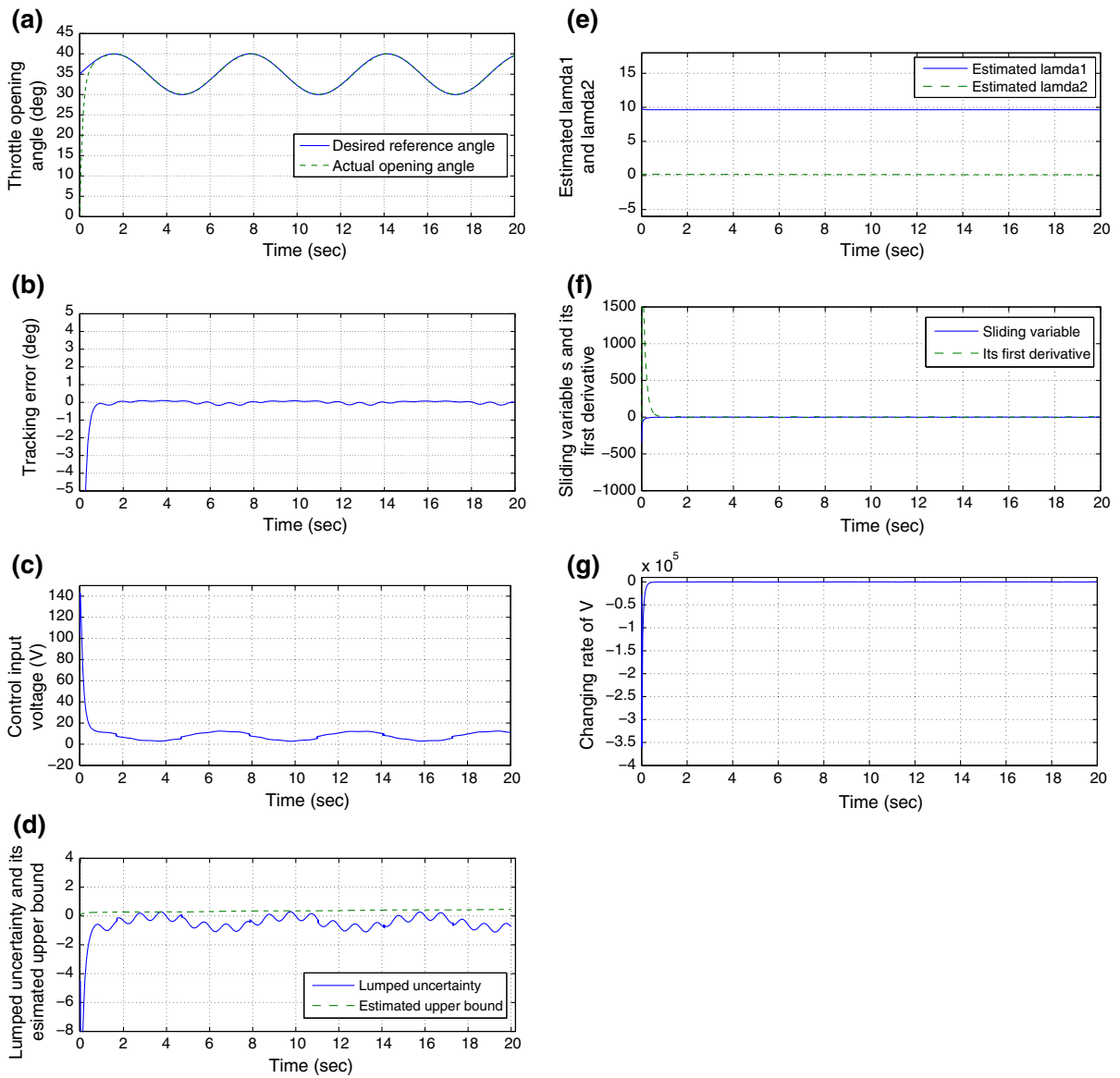


Fig. 6 Control performance of RASM control in Case 2. **a** Tracking performance. **b** Tracking error. **c** Control voltage. **d** Lumped uncertainty and its estimated upper bound. **e** Estimated gains $\hat{\lambda}_1$

and $\hat{\lambda}_2$. **f** Sliding variable s and its first derivative. **g** Changing rate of Lyapunov function V

ing errors under the PID and H_∞ controllers in Case 1. We can see that although the PID control achieves the similar steady-state error to the proposed control except the starting period (2 s), the settling time of 1 s is more than double the time by the proposed control. For the H_∞ control, although its setting time is smaller than the one of the proposed control and PID control, it has

about 2° steady-state error when the throttle operates from 40° to 70°.

In order to test the robustness of the three controllers under sinusoidal tracking purpose, Figs. 6, 7 and 8 demonstrate the tracking performance of the closed-loop ET system for sinusoidal reference angle under parameter variations and external disturbances in Case

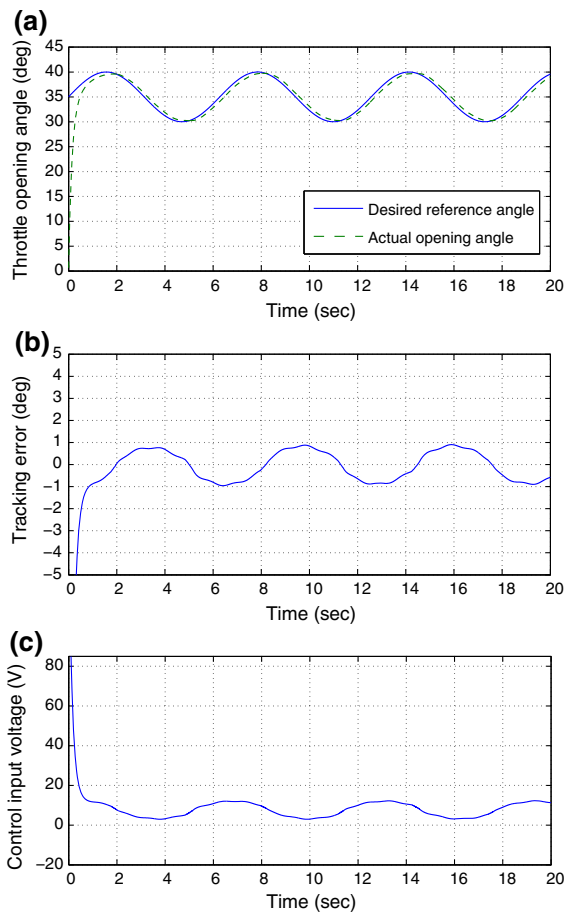


Fig. 7 Control performance of PID control in Case 2. **a** Tracking performance. **b** Tracking error. **c** Control voltage

2. It is observed that the tracking precision with the proposed RASM control in Fig. 6 is much better than the ones with the PID and H_∞ controllers in Figs. 7 and 8. We can see that the proposed control achieves the smallest steady-state tracking error bound (TEB) of 0.4 deg, while the values of TEB of the PID and H_∞ control are around 1.0° and 1.1°, respectively. In addition, the estimated lumped uncertainty bound $\hat{\eta}$, and the control gains $\hat{\Lambda}_1$ and $\hat{\Lambda}_2$ are all adaptively adjusted as the sliding mode parameters in the sense that the sliding variable can converge to zero and after that, they become certain constants to guarantee the closed-loop stability condition. Due to the fact that proposed RASM control with the adaptive laws for the lumped certainty bound and the two control gains can eliminate the effects of the parametric variations and external disturbances on the throttle tracking performance, the proposed con-

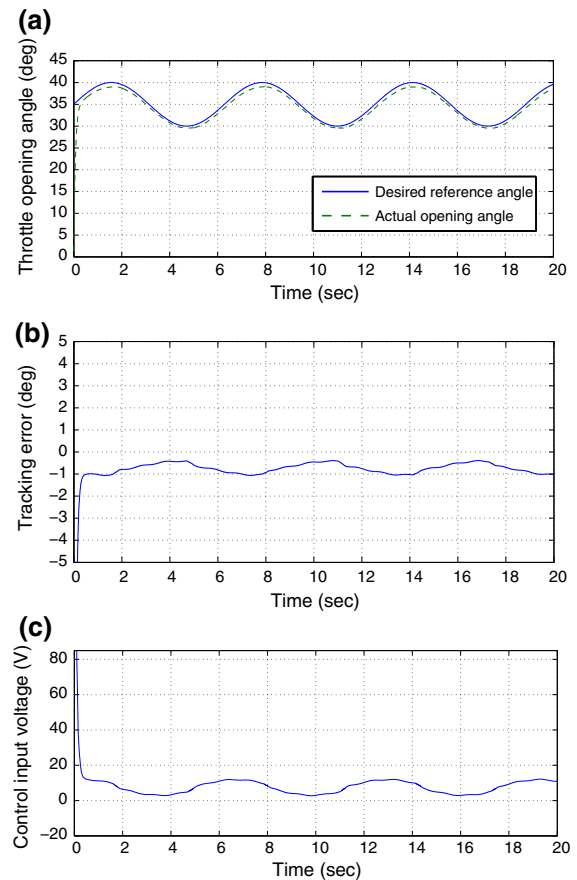


Fig. 8 Control performance of H_∞ control in Case 2. **a** Tracking performance. **b** Tracking error. **c** Control voltage

trol is thus capable of achieving a stronger robustness against uncertainties than the ones of the conventional PID and H_∞ control methods.

5 Experimental results

In this section, in order to verify the effectiveness of the proposed control, we carry out a series of DC motor-based hardware-in-loop experiments. It is seen from Fig. 9 that, a brushless DC motor is connected with a gearhead and an encoder installed inside the motor is used to provide with the angular velocity and position information of the motor shaft.

Although there are no mechanical loads of the throttle valve plate and gears included due to the hardware limitation, the robust control performance of the pro-

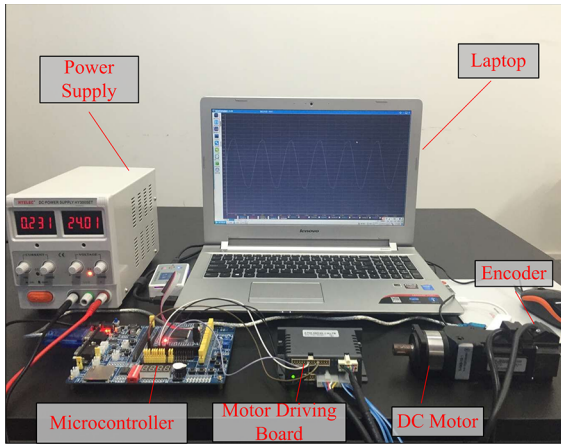


Fig. 9 Image of hardware-in-loop experimental system

Table 2 Control parameters of the proposed and PID control in experiments

Parameter	Value
ξ_1	1500
ξ_2	5
ξ_3	5
ξ_4	0.1
k	0.01
$\hat{\eta}(0)$	1000
$\hat{\Lambda}_1(0)$	100
$\hat{\Lambda}_2(0)$	100
k_p	-5600
k_i	-10
k_d	-3

posed control can still be validated by imposing an equivalent electronic voltage signal to the system once the experiments start, as $V_{\tau_L} = 0.45 \sin(0.2t)$.

Please note that the control algorithms are implemented on a Freescale microcontroller (MCU) board (MC9S12XEP100) using the “C” languages using CodeWarrior Development Studio V5.1 from Metrowerks incorporated in a laptop and downloaded to the MCU. The control voltage is given in the form of pulse width modulation (PWM) with the frequency of 3.2 kHz. The sampling period is chosen as 10 ms.

In this section, we carry out the experiments under the proposed control and the PID control only for comparison and the corresponding parameters are listed in Table 2.

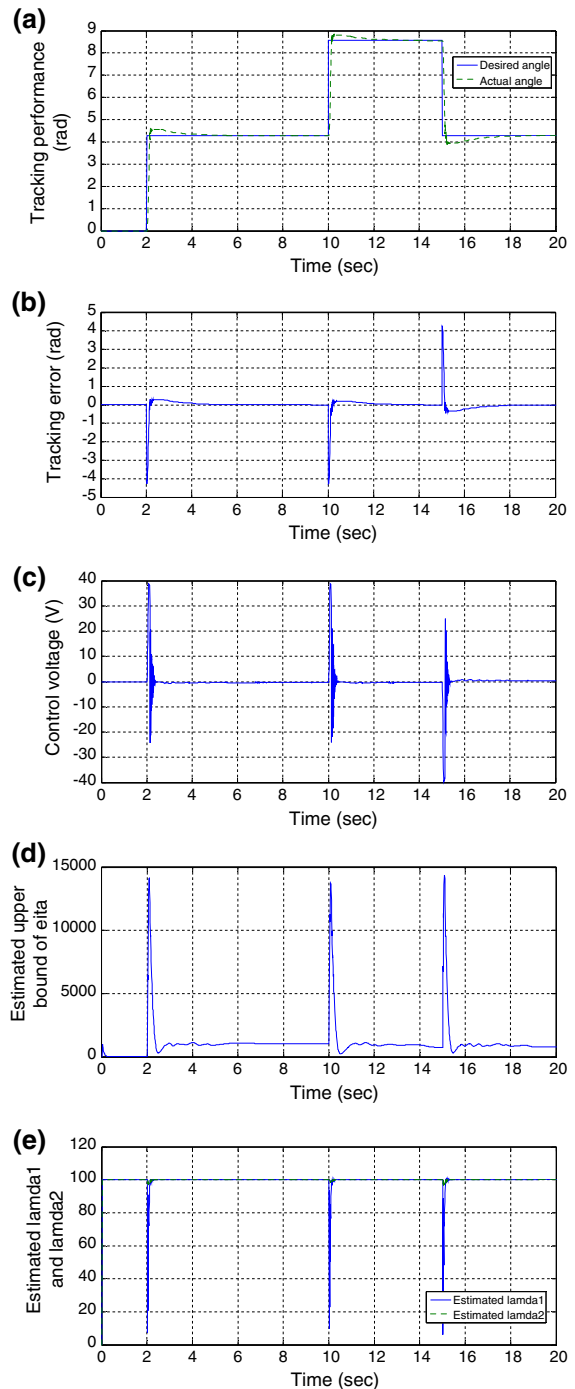


Fig. 10 Control performance of RASM control at Case 1 in experiments. **a** Tracking performance. **b** Tracking error. **c** Control voltage. **d** Estimated upper bound of lumped uncertainty. **e** Estimated gains $\hat{\Lambda}_1$ and $\hat{\Lambda}_2$

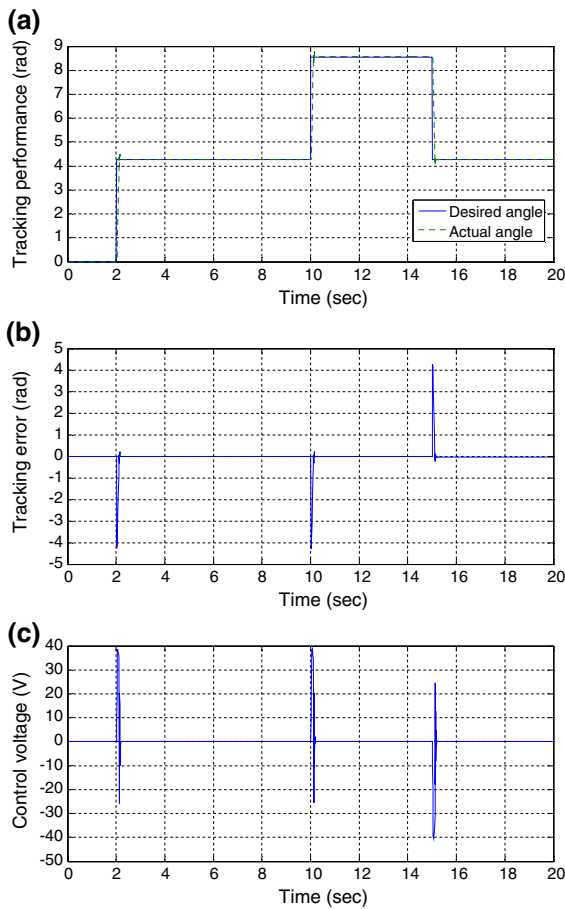


Fig. 11 Control performance of PID control at Case 1 in experiments. **a** Tracking performance. **b** Tracking error. **c** Control voltage

The experimental results of the two controllers for Cases 1 and 2 are shown in Figs. 10, 11, 12 and 13. It is observed that although the PID control presents a smaller overshoot than the proposed control at Case 1, the smaller steady-state error of the proposed control is achieved compared with the PID counterpart particularly from 12 to 15 s. Moreover, the proposed control exhibits an apparently smaller tracking error compared with the PID control under the disturbances at Case 2. It thus indicates that the proposed RASM control performs very well and behaves with a strong robustness against the changes of the reference commands and the external disturbances.

It should be noted from Fig. 12 that, the chattering occurring in the first 0.5 s is caused by the adaption process of the proposed RASM control in order to alleviate the effects of the external disturbance. After that,

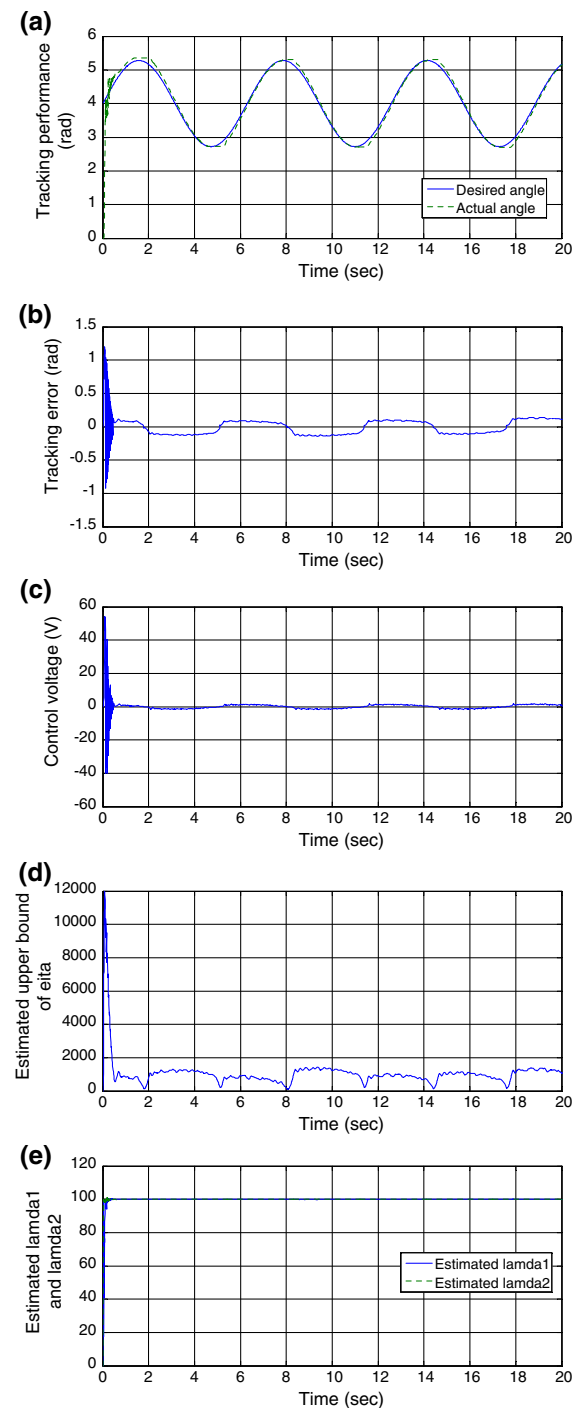


Fig. 12 Control performance of RASM control at Case 2 in experiments. **a** Tracking performance. **b** Tracking error. **c** Control voltage. **d** Estimated upper bound of lumped uncertainty. **e** Estimated gains $\hat{\lambda}_1$ and $\hat{\lambda}_2$

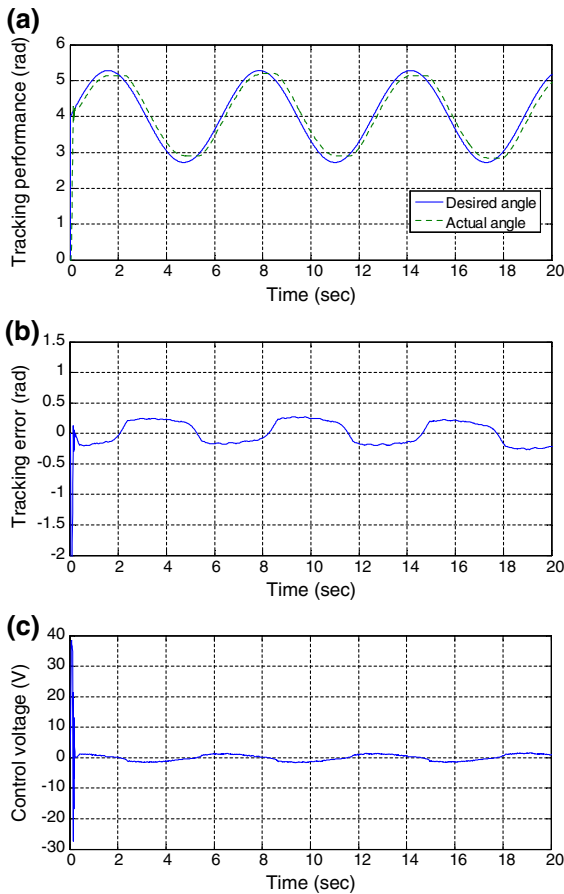


Fig. 13 Control performance of PID control at Case 2 in experiments. **a** Tracking performance. **b** Tracking error. **c** Control voltage

it is clearly seen that the control smoothness can be guaranteed until the experiments stop.

6 Conclusion

In this paper, the RASM control scheme for automotive ET systems has been proposed. It has been demonstrated that the proposed control can achieve a fast and robust tracking performance. Both the lumped uncertainty bound and the control gains are adaptively adjusted using update laws such that the requirements of the information of the uncertainty and control gains can be released. Both the simulation and experimental results have verified the validity and the excellent tracking performance of the proposed control, in comparison with PID and H_∞ controllers. The future research work

to design a super-twisting sliding mode control scheme with an uncertainty observer for ET systems is under the authors' investigation.

Acknowledgments This research was supported by the National Nature Science Foundation of China (No. 61503113).

References

- Zito, G., Tona, P., Lassami, B.: The throttle control benchmark. In: Proceedings of E-COSM, IFAC Workshop Engine Powertrain Control, Simulation, Modelling, Rueil-Malmaison, France, pp. 1–2 (2009)
- Aono, T., Kowatari, T.: Throttle-control algorithm for improving engine response based on air-intake model and throttle-response model. *IEEE Trans. Ind. Electron.* **53**(3), 915–921 (2006)
- Deur, J., Pavkovic, D., Peric, N., Jansz, M., Hrovat, D.: An electronic throttle control strategy including compensation of friction and limp-home effects. *IEEE Trans. Ind. Appl.* **40**(3), 821–834 (2004)
- Alt, B., Blath, J.P., Svaricek, F., Schultalbers, M.: Self-tuning control design strategy for an electronic throttle with experimental robustness analysis. In: Proceedings of American Control Conference, pp. 6127–6132 (2010)
- Grepl, R., Lee, B.: Modeling, parameter estimation and nonlinear control of automotive electronic throttle using a rapid-control prototyping technique. *Int. J. Autom. Technol.* **11**(4), 601–610 (2010)
- Vasak, M., Baotic, M., Morari, M., Petrovic, I., Peric, N.: Constrained optimal control of an electronic throttle. *Int. J. Control* **79**(5), 465–478 (2006)
- Vasak, M., Baotic, M., Petrovic, I., Peric, N.: Hybrid theory-based time-optimal control of an electronic throttle. *IEEE Trans. Ind. Electron.* **54**(3), 1483–1494 (2007)
- Yuan, X., Wang, Y.: Neural networks based self-learning PID control of electronic throttle. *Nonlinear Dyn.* **55**(4), 385–393 (2009)
- Yuan, X., Wang, Y., Sun, W., Wu, L.: RBF networks-based adaptive inverse model control system for electronic throttle. *IEEE Trans. Veh. Technol.* **59**(8), 3757–3765 (2010)
- Jansri, A., Pongsuttiyakorn, T., Sooraksa, P.: On practical control of electronic throttle body. In: Proceedings of 9th Int. Conf. Fuzzy Syst. Knowl. Discov., pp. 349–351 (2012)
- Wang, C.H., Huang, D.Y.: A new intelligent fuzzy controller for nonlinear hysteretic electronic throttle in modern intelligent automobiles. *IEEE Trans. Ind. Electron.* **60**(16), 2332–2345 (2013)
- Pavkovic, D., Deur, J., Jansz, M., Peric, N.: Adaptive control of automotive electronic throttle. *Control Eng. Pract.* **14**(2), 121–136 (2006)
- Pozo, F., Acho, L., Vidal, Y.: Nonlinear adaptive tracking control of an electronic throttle system: benchmark experiments. In: Proceedings of E-COSM IFAC Workshop Engine Powertrain Control, Simulation, Modelling, Rueil-Malmaison, France (2009)
- Bernardo, M., Gaeta, A., Montanaro, U., Santini, S.: Synthesis and experimental validation of the novel LQ-NEMCSI

- adaptive strategy on an electronic throttle valve. *IEEE Trans. Control Syst. Technol.* **18**(6), 1325–1337 (2010)
15. Jiao, X., Zhang, J., Shen, T.: An adaptive servo control strategy for automotive electronic throttle and experimental validation. *IEEE Trans. Ind. Electron.* **61**(11), 6275–6284 (2014)
 16. Wang, H., Kong, H., Man, Z., Do, M.T., Cao, Z., Shen, W.: Sliding mode control for steer-by-wire systems with AC motors in road vehicles. *IEEE Trans. Ind. Electron.* **61**(3), 1596–1611 (2014)
 17. Wang, H., Man, Z., Shen, W., Cao, Z., Zheng, J., Jin, J., Do, M.T.: Robust control for steer-by-wire systems with partially known dynamics. *IEEE Trans. Ind. Inform.* **10**(4), 2003–2015 (2014)
 18. Zheng, J., Wang, H., Man, Z., Jin, J., Fu, M.: Robust motion control of a linear motor positioner using fast nonsingular terminal sliding mode. *IEEE Trans. Mechatron.* **20**(4), 1743–1752 (2015)
 19. Edwards, C., Spurgeon, S.: *Sliding Mode Control: Theory and Applications*. Taylor & Francis, New York (1998)
 20. Pai, M.C.: Dynamic output feedback RBF neural network sliding mode control for robust tracking and model following. *Nonlinear Dyn.* **79**(2), 1023–1033 (2015)
 21. Liu, L., Pu, J., Song, X., Fu, Z., Wang, X.: Adaptive sliding mode control of uncertain chaotic systems with input nonlinearity. *Nonlinear Dyn.* **76**(4), 1857–1865 (2014)
 22. Mobayen, S.: Design of CNF-based nonlinear integral sliding surface for matched uncertain linear systems with multiple state-delays. *Nonlinear Dyn.* **77**(3), 1047–1054 (2014)
 23. Mobayen, S.: Fast terminal sliding mode controller design for nonlinear second-order systems with time-varying uncertainties. *Complexity* (2014). doi:[10.1002/cplx.21600](https://doi.org/10.1002/cplx.21600)
 24. Mobayen, S.: Finite-time stabilization of a class of chaotic systems with matched and unmatched uncertainties: an LMI approach. *Complex* (2014). doi:[10.1002/cplx.21624](https://doi.org/10.1002/cplx.21624)
 25. Mobayen, S.: Finite-time tracking control of chained-form nonholonomic systems with external disturbances based on recursive terminal sliding mode method. *Nonlinear Dyn.* **80**(1), 669–683 (2015)
 26. Mobayen, S.: Fast terminal sliding mode tracking of nonholonomic systems with exponential decay rate. *IET Control Theory Appl.* **9**(8), 1294–1301 (2015)
 27. Mobayen, S.: An adaptive fast terminal sliding mode control combined with global sliding mode scheme for tracking control of uncertain nonlinear third-order systems. *Nonlinear Dyn.* **82**(1), 599–610 (2015)
 28. Pan, Y., Ozguner, U., Dagci, O.H.: Variable-structure control of electronic throttle valve. *IEEE Trans. Ind. Electron.* **55**(11), 3899–3907 (2008)
 29. Reichhartinger, M., Horn, M.: Application of higher order sliding mode concepts to a throttle actuator for gasoline engines. *IEEE Trans. Ind. Electron.* **56**(9), 3322–3329 (2009)
 30. Shieh, N.C.: Robust output tracking control of a linear brushless DC motor with time-varying disturbances. *IEE Proc. Electr. Power Appl.* **149**(1), 39–45 (2002)